Analysis of Parametric Decay Instabilities Driven by Helicon Waves in Tokamak Experiments

Xiaoyu Yang[1*], and *Zhe* Gao[1]

[1]Department of Engineering Physics, Tsinghua University, 100084 Beijing, China

Abstract. In this study, we analyse and compute the local growth rate of parametric decay instabilities of helicon waves under typical scrape-off layer conditions. Our findings are consistent with previous work [Porkolab et al., AIP Conference Proceedings **2984**, 070004 (2023)], confirming that the dominant decay channels are ion cyclotron quasi-modes and their harmonics. While the parametric instability can be excited at extremely low input power, it can be suppressed by a higher electron temperature. Conversely, higher plasma densities increase the local growth rate, suggesting that helicon waves may face challenges in high-density plasmas.

1 Introduction

Helicon waves, the fast wave branch in the lower hybrid frequency range, have been employed in tokamak devices [1,2] and attracted growing interest as candidates for non-inductive current drive method [3–6]. They are predicted by simulations to offer several advantages, including better accessibility and strong single-pass damping in high β_e tokamaks [7]. However, although it is predicted that helicon waves may undergo less nonlinear parametric decay instabilities (PDIs) due to their lower effective electric field [3], experimental observations still reveal traces of PDIs [1], raising concerns about potential unanticipated power loss in the scrape-off layer (SOL).

In the DIII-D experiment [1], spectral broadening and enhancement at sidebands were observed, which were interpreted as parametric decay instabilities, and no clear threshold for PDI excitation was observed. A subsequent theoretical analysis by Porkolab et al. [8] calculated the PDI spectrum and proposed ion cyclotron quasi-modes as the dominant decay channels.

A recently developed kinetic theory-based framework for PDIs [9] features a simplified kinetic-fluid hybrid approach, which is capable of modeling the decay of a pump wave into two quasi-electrostatic waves. Unlike the model in [8], this approach retains the full electromagnetic dispersion relation of the pump wave and can derive nonlinear coupling effects through an iterative procedure. This framework can also be extended to future nonlocal analyses, providing a more versatile foundation for studying PDI saturation.

In this work, we revisit the problem using this kinetic-fluid hybrid method to benchmark Porkolab's results and analyse the parameter dependence of the local PDI growth rate. Section 2 briefly outlined the kinetic-fluid hybrid model used in this study. Section 3 presents the typical PDI spectra and analyses the parameter dependence of the PDI local growth rate. Section 4 gives the discussion, addressing the future challenges of helicon wave applications in tokamaks.

2 Theoretical Model

A homogeneous plasma system with a background magnetic field $\boldsymbol{B}_0$ along the z -direction is adopted. The pump helicon wave is the fast wave branch of lower hybrid frequency with linear dispersion relation [7]

$$N_\perp^2 = \frac{(S-N_z^2)^2-D^2}{S-N_z^2}. \tag{1.1}$$

Here, $S = 1 - \sum_s \frac{\omega_{ps}^2}{\omega_0^2-\omega_{cs}^2}$, $D = \sum_s \frac{\omega_{cs}\omega_{ps}^2}{\omega_0(\omega_{cs}^2-\omega_0^2)}$, ω_{ps} is the plasma frequency, ω_{cs} is the cyclotron frequency, where the subscript s denotes the particle species. And the $N = \frac{c}{\omega_0}k$ means the wave vector normalized by the pump frequency ω_0.

We consider a pump helicon wave $(\omega_0, \boldsymbol{k}_0)$ decay into a lower hybrid wave as sidemode $(\omega_1, \boldsymbol{k}_1)$ and an ion wave as low-frequency mode $(\omega_{\mathrm{LF}}, \boldsymbol{k}_{\mathrm{LF}})$. The frequency and wave vector satisfy the phase matching conditions,

$$\begin{aligned} \omega_{\mathrm{LF}} &= \omega_0 + \omega_1, \\ \boldsymbol{k}_{\mathrm{LF}} &= \boldsymbol{k}_0 + \boldsymbol{k}_1. \end{aligned} \tag{1.2}$$

The linear behaviour of the wave is described by the kinetic model and the linear perturbed density is [9]

$$n_{s,j}^L = \frac{\chi_{s,j}^L \varepsilon_0 k_j^2}{e}\phi_j. \tag{1.3}$$

Here, the $j = \mathrm{LF}$, $0, 1$ represents the pump, sideband or the low-frequency wave. $\chi_{s,j}$ is the linear susceptibility under potential $\phi_j = exp\left[-i\left(\omega_j t - \boldsymbol{k}_j \cdot \boldsymbol{x}\right)\right]$,

$$\chi_{s,j}^L = \frac{2\omega_{ps}^2}{k_j^2 v_s^2}\left[1 + \frac{\Omega}{k_{jz}v_s}\sum_{l=-\infty}^{+\infty} Z(\xi_j) I_l(b_{sj}) e^{-b_{sj}}\right], \tag{1.4}$$

* Corresponding author: yang-xy19@mails.tsinghua.edu.cn

where the $v_s = \sqrt{2T_s/m_s}$ is the thermal velocity, $Z(\xi_l)$ is the plasma dispersion function with $\xi_l = (\omega_j - l|\omega_{cs}|)/k_{jz}v_s$, and $I_l(b_{sj})$ is the modified Bessel function with $b_{sj} = k_{j\perp}^2 v_s^2/2\omega_{cs}^2$.

While the linear response is derived from kinetic theory, the nonlinear response can be approximated by the fluid theory. The nonlinear electron density arises from the ponderomotive force, and the resulting ponderomotive potential is given by [9],

$$\phi_{\rm pe} = \frac{e\phi_0\phi_1}{2m_e k_{sz}}\left[i\frac{(\boldsymbol{k}_{0\perp}\times\boldsymbol{k}_{1\perp})}{\omega_{\rm ce}}\left(\frac{k_{0z}}{\omega_1} - \frac{k_{1z}}{\omega_0}\right) + k_{1z}k_{0z}\left(\frac{k_{0z}}{\omega_1^2} + \frac{k_{1z}}{\omega_0^2}\right)\right]. \quad (1.5)$$

The nonlinear coupling equation for the low-frequency mode is easily obtained by using Poisson's equation,

$$\varepsilon_{\rm LF}^L\phi_{\rm LF} = -\frac{e}{2m_e k_{{\rm LF},z}}\chi_{e,{\rm LF}}^L\left[i\frac{(\boldsymbol{k}_{0\perp}\times\boldsymbol{k}_{1\perp})\cdot z}{\omega_{\rm ce}}\left(\frac{k_{0z}}{\omega_1} - \frac{k_{1z}}{\omega_0}\right) + k_{1z}k_{0z}\left(\frac{k_{0z}}{\omega_1^2} + \frac{k_{1z}}{\omega_0^2}\right)\right]\phi_0\phi_1. \quad (1.6)$$

Here, $\varepsilon_{\rm LF}^L = 1 + \chi_{e,{\rm LF}}^L + \chi_{i,{\rm LF}}^L$ is the dielectric function of the low-frequency mode.

For the sideband, the coupling equation can be obtained through fluid continuity equation,

$$\varepsilon_1\phi_1 = -\frac{ek_{\rm LF}^2(\chi_{e,{\rm LF}}^L - \varepsilon_{\rm LF}^L)}{2\omega_1 m_e k_1^2}\left[i\frac{(\boldsymbol{k}_{1\perp}\times\boldsymbol{k}_{0\perp})\cdot z}{\omega_{\rm ce}^2} - \frac{k_{0z}k_{1z}}{\omega_0}\right]\phi_{\rm LF}\phi_0^*. \quad (1.7)$$

The dispersion relation of PDI driven by helicon wave is obtained by coupling and solving Eqs.(1.6) and (1.7),

$$\varepsilon(\omega_{\rm LF}, \boldsymbol{k}_{\rm LF}) - \frac{\mu_1}{\varepsilon_1(\omega_{\rm LF}-\omega_0, \boldsymbol{k}_{\rm LF}-\boldsymbol{k}_0)} = 0, \quad (1.8)$$

where μ_1 is the coupling coefficient of PDI process,

$$\mu_1 = \frac{\omega_{pi}^4|u_0|^2}{4\omega_0^2 k_{LF}^2 c_s^4}\frac{\chi_{e,{\rm LF}} - \varepsilon_{e,{\rm LF}}}{\chi_{e,{\rm LF}}}[1 + \xi_{LF}Z(\xi_{LF})]^2\left(sin^2\,\delta + \frac{|\omega_{ce}|k_{0z}k_{1z}}{\omega_0|\mathbf{k}_{0\perp}||\mathbf{k}_{1\perp}|}\right). \quad (1.9)$$

Here the $\xi_{\rm LF} = \omega_{\rm LF}/k_z v_e$, $u_0 = k_{0\perp}\phi_0/B_0$ is the drift velocity, $c_s = \sqrt{T_e/m_i}$ is the ion sound speed, δ is the angle between $\boldsymbol{k}_{0\perp}$ and $\boldsymbol{k}_{1\perp}$. By solving Eq. (1.8), we can compute the frequency-wavenumber relationship of the low-frequency mode, which then allow us to get the growth rate and frequency of the low-frequency mode.

3 Decay channel analysis and parameter dependence

3.1 Decay channel analysis

The parameters are chosen the same as in [8], where $B_0 = 1.4$ T, $n_e = 3\times10^{18}$ m^{-3}, $f_0 = 476$ MHz, $N_{0z} = 3$, $T_e = 50$ eV, $T_i = 200$ eV, $N_{1z} = 8$ and $P_0 = 0.3$ MW. For numerical computation, the angle δ between $\boldsymbol{k}_{0\perp}$ and $\boldsymbol{k}_{1\perp}$ also needs to be fixed. Here, we have selected a representative value of 90° for illustrative purposes. By calculating the growth rate and real frequency of the low-frequency mode while changing the perpendicular wavenumber $N_{{\rm LF},\perp}$, the PDI spectrum is obtained and shown in Fig. 1.

Clearly, the maxima of the growth rate arise near the ion cyclotron frequency and its harmonics, with the peak growth rate occurring at the third harmonic ($\omega_{{\rm LF},r} = 3\omega_{\rm ci}$). These computational results show agreement with [8], confirming ion cyclotron quasi-modes (ICQM) as the dominant decay channel. However, the results also show that the low-frequency ion sound quasi-mode (ISQM) can exist as a decay channel, which is seen from the lower left of Fig. 1. The growth rate of the ISQM decay is significantly weaker than that of ICQMs, making its contribution to overall parametric decay negligible. This might explain why strong sidebands appear in the experimental RF spectrum, while the pump wave exhibits only a slight broadening.

Moreover, our calculation of PDI spectrum under low pump power conditions demonstrates that the local growth rate persists even at significantly reduced power levels (0.01 MW, Fig. 2). Although the ICQMs remain the primary decay channel, their local growth rate shows significant reduction.

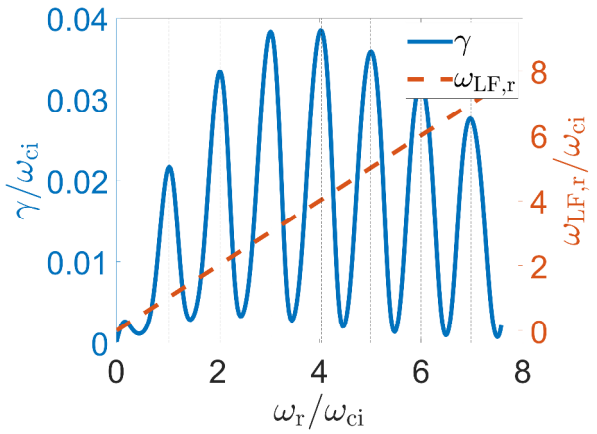

Fig. 1. The real part of frequency $\omega_{\rm LF,r}$ (the red curve) and the temporal growth rate $\gamma_{\rm LF}$ (the blue curve) are shown as functions of the frequency $\omega_{\rm LF,r}$.

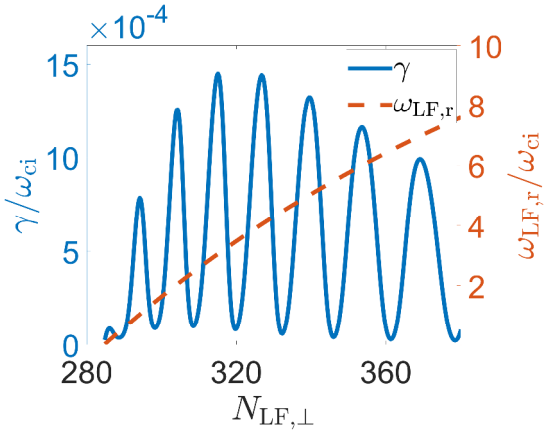

Fig. 2 The real part of frequency $\omega_{\rm LF,r}$ (the red curve) and the temporal growth rate $\gamma_{\rm LF}$ (the blue curve) are shown as functions of the wavenumber $N_{\rm LF,\perp}$. The pump power is changed to 0.01 MW.

3.2 Scattering angle δ dependence

In the preceding subsection, the scattering angle δ was fixed at 90° to demonstrate a typical condition. However, a careful scan is required to determine appropriate representative value for δ.

We evaluate the PDI strength using the maximum value γ_{max} across the entire growth rate curve, and then calculate its variation with δ. As shown in Fig. 3, γ_{max} increases monotonically with δ, peaking at 90°. This trend can be derived from the coupling coefficient Eq.(1.9), where δ is primarily manifested in the $sin^2\,\delta$ term while slightly affect the value of $k_{0\perp}$ and $k_{\mathrm{LF},\perp}$ through the phase matching condition.

3.3 Plasma temperature T_e dependence

Consistent with previous findings for LHWs [10,11], our results of helicon waves demonstrate that electron temperature suppresses the PDI.

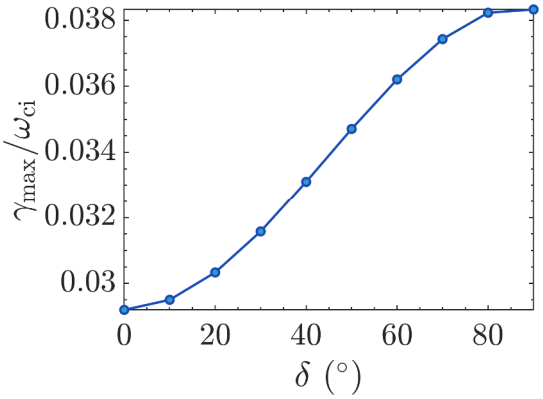

Fig. 3. The growth rate $\gamma/\omega_{\mathrm{ci}}$ dependence on δ, when $B_0 = 1.4\,\mathrm{T}$, $n_e = 3\times10^{18}\,\mathrm{m}^{-3}$, $f_0 = 476\,\mathrm{MHz}$, $N_{0z} = 3$, $T_e = 50\,\mathrm{eV}$, $T_i = 200\,\mathrm{eV}$, $N_{1z} = 8$ and $P_0 = 0.3\,\mathrm{MW}$. Here, γ_{max} is taken as the maximum value across the entire PDI growth rate spectrum.

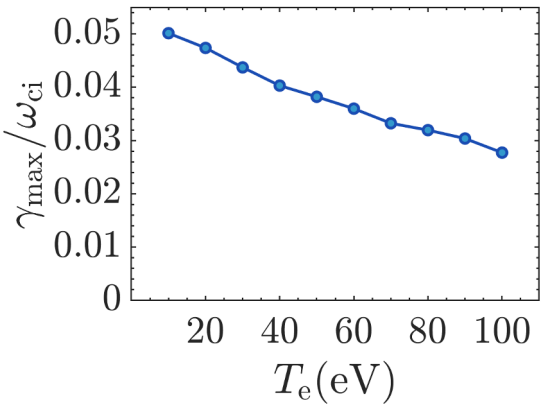

Fig. 4. The dependence of the maximum growth rate γ_{max} on electron temperature, when $B_0 = 1.4\,\mathrm{T}$, $n_e = 3\times10^{18}\,\mathrm{m}^{-3}$, $f_0 = 476\,\mathrm{MHz}$, $N_{0z} = 3$, $T_i = 200\,\mathrm{eV}$, $N_{1z} = 8$, $P_0 = 0.3\,\mathrm{MW}$ and $\delta = 90^{\circ}$. Here, γ_{max} is taken as the maximum value across the entire PDI growth rate spectrum.

Fig. 4 reveals a clear reduction in the maximum growth rate γ_{max} with increasing SOL electron temperature. This stabilizing effect arises because higher temperatures weaken the wave coupling process by increasing the c_s term in Eq. (1.9).

3.4 Plasma density n_e dependence

The plasma density dependence is presented in Fig.5. The local growth rate increases with increasing density, which mirrors the trend observed in ICQM calculations for LHWs [11]. This agreement further confirms that the helicon-driven PDIs are also dominated by ISQMs. Moreover, the observed density dependence suggests that helicon waves might encounter a similar density limit problem as LHWs due to the enhanced boundary losses at high densities.

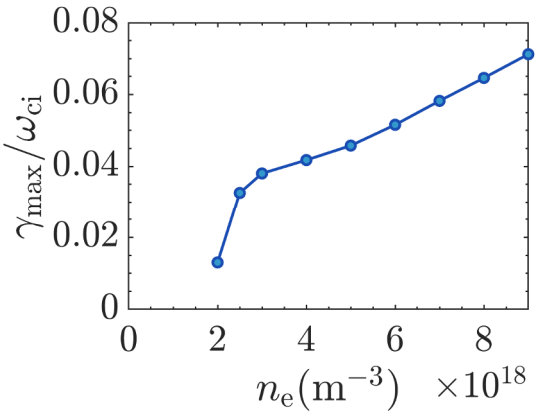

Fig. 5. The dependence of the maximum growth γ_{max} rate on electron density n_e, when $B_0 = 1.4\,\mathrm{T}$, $f_0 = 476\,\mathrm{MHz}$, $N_{0z} = 3$, $T_e = 50\,\mathrm{eV}$, $T_i = 200\,\mathrm{eV}$, $N_{1z} = 8$ and $P_0 = 0.3\mathrm{MW}$ and $\delta = 90^{\circ}$. Here, γ_{max} is taken as the maximum value across the entire PDI growth rate spectrum.

4 Discussion

This work elucidates the dominant decay channels of helicon wave-driven PDI. The analysis reveals that pump helicon waves primarily decay into lower hybrid waves and ion cyclotron quasi-modes, in agreement with both DIII-D experimental observations [1] and Porkolab's theoretical calculations [8].

Parameter dependence analysis demonstrates that the maximum PDI growth rate occurs under perpendicular scattering conditions. While a higher electron temperature exhibits a stabilizing effect by suppressing PDI intensity, an increased plasma density enhances the PDI growth rate. This density dependence reveals that the density limit problem may also happen during helicon wave injection.

The emergence of low-threshold PDI also provides partial validation that PDIs are common phenomena in helicon current drive experiments. However, the precise threshold for this instability requires further investigation through non-local simulations incorporating additional damping mechanisms [12–14], which will be presented in our future work.

References

1. R.I. Pinsker, B. Van Compernolle, S.X. Tang, J.B. Lestz, C.P. Moeller, C.C. Petty, A. Dupuy, J.P. Squire, A.M. Garofalo, M. Porkolab, J.C. Rost, S.G. Baek, A. Nagy, S. Chowdhury, N.A. Crocker, G.H. Degrandchamp, A.G. McLean, K.R. Gage, A. Marinoni, E.H. Martin, G. Ronchi, and the D.-D. Team, First high-power helicon results from DIII-D, Nuclear Fusion **64**, 126058 (2024). https://doi.org/10.1088/1741-4326/ad78e8
2. H.Y. Lee, J.H. Kim, H.H. Wi, J.G. Kwak, and S.J. Wang, RF conditioning to suppress multipactor discharge for helicon wave current drive in KSTAR, Fusion Engineering and Design **193**, 113782 (2023). https://doi.org/10.1016/j.fusengdes.2023.113782
3. V.L. Vdovin, Current generation by helicons and lower hybrid waves in modern tokamaks and reactors ITER and DEMO. Scenarios, modeling and antennae, Plasma Phys. Rep. **39**, 95 (2013). https://doi.org/10.1134/S1063780X13020037
4. X. Li, H. Liu, N. Xiang, and M. Li, Theoretical analysis of helicon wave current drive in EAST with high β_e operation, Physics Letters A **384**, 126779 (2020). https://doi.org/10.1016/j.physleta.2020.126779
5. H.B. Liu, X.X. Li, Z.Y. Xiao, D.Z. Zhang, and A.P. Sun, Numerical simulation of helicon waves current drive in the HL-2M tokamak for the steady-state scenario, J. Korean Phys. Soc. **79**, 1135–1140 (2021). https://doi.org/10.1007/s40042-021-00326-5
6. M.A. Irzak, and S.A. Nechaev, Full-Wave 2D Modeling of Helicons Propagation and Absorption in the Spherical Tokamak Globus-M2, Tech. Phys. **68**, 361 (2023). https://doi.org/10.1134/S1063784223900644
7. C. Lau, E.F. Jaeger, N. Bertelli, L.A. Berry, D.L. Green, M. Murakami, J.M. Park, R.I. Pinsker, and R. Prater, AORSA full wave calculations of helicon waves in DIII-D and ITER, Nucl. Fusion **58**, 066004 (2018). https://doi.org/10.1088/1741-4326/aab96d
8. M. Porkolab, R.I. Pinsker, G.H. DeGrandchamp, S.G. Baek, B.V. Compernolle, S. Denk, C.C. Petty, S.X. Tang, and K.E. Thome, Parametric decay instabilities driven by high power helicon waves in DIII-D, AIP Conference Proceedings **2984**, 070004 (2023). https://doi.org/10.1063/5.0163570
9. Z. Gao, Z.H. Su, Z.R. Liu, Z.K. Huang, J.Y. Han, and Z.Y. Liu, Kinetic theory of parametric instabilities in magnetized plasmas and its application to analyzing decay waves during the injection of lower hybrid waves, Nucl. Fusion **65**, 046033 (2025). https://doi.org/10.1088/1741-4326/adbcc4
10. R. Cesario, L. Amicucci, A. Cardinali, C. Castaldo, M. Marinucci, F. Napoli, F. Paoletti, D. De Arcangelis, M. Ferrari, A. Galli, G. Gallo, E. Pullara, G. Schettini, and A.A. Tuccillo, Spectral broadening of parametric instability in lower hybrid current drive at a high density, Nucl. Fusion **54**, 043002 (2014). https://doi.org/10.1088/0029-5515/54/4/043002
11. A. Zhao, and Z. Gao, Parameter study of parametric instabilities during lower hybrid wave injection into tokamaks, Nucl. Fusion **53**, 083015 (2013). https://doi.org/10.1088/0029-5515/53/8/083015
12. K. Chen, and Z. Gao, Saturation of a quasi-mode parametric instability in an inhomogeneous plasma, Nucl. Fusion **65**, 036020 (2025). https://doi.org/10.1088/1741-4326/adb0de
13. K. Chen, and Z. Gao, Analysis of the convective amplification process of a three-wave parametric instability arises from low frequency plasma fluctuation, Plasma Phys. Control. Fusion **67**, 035026 (2025). https://doi.org/10.1088/1361-6587/adb888
14. K. Chen, and Z. Gao, Absolute parametric instabilities with non-resonant daughter waves in an inhomogeneous plasma, Commun. Theor. Phys. **77**, 115501 (2025). https://doi.org/10.1088/1572-9494/addb26